The Electrochemical Society
Advancing solid state & electrochemical science & technology

Electrochemical Properties of Composite Cathode Using Bimodal Sized Electrolyte for All-Solid-State Batteries

To cite this article: Chanhwi Park *et al* 2019 *J. Electrochem. Soc.* **166** A5318

Electrochemical Properties of Composite Cathode Using Bimodal Sized Electrolyte for All-Solid-State Batteries

Chanhwi Park, Sangsoo Lee, Kyubeom Kim, Minhee Kim, Sunho Choi, and Dongwook Shin [ID][z]

Division of Materials Science & Engineering, Hanyang University, Seongdong-gu, Seoul 04763, Korea

To enhance the packing density of composite cathode for all-solid-state lithium-ion batteries, the effect of a bimodal sized solid electrolyte was studied. The composite cathode, which is fabricated using the powder compression method, consisted of the cathode active material, a conductive agent, and the solid electrolyte. However, the composite cathode construction had voids. The voids in the composite cathode were restricted to ionic conduction between the cathode active materials and the solid electrolytes. Suppression of the voids in the composite cathode improved the electrochemical performance of the all-solid-state battery. A composite cathode using bimodal sized electrolyte powders demonstrated better cell performance than that using only fine or coarse sized electrolyte powders. These results demonstrated that the composite cathode using the bimodal sized electrolyte enhanced the electrochemical performance of the all-solid-state battery because it improved the packing density of the cathode.

Today, the demand for rechargeable power sources with a high energy density is increasing due to the spread of electrification. Rechargeable lithium ion batteries (LIBs) is a high energy density power source that have been used as a power sources in electric devices.[1] Thus, the demand for large scale LIBs used in electric vehicles (EV) and energy storage systems (ESS) has been increasing. However, the safety issues, which scale proportionally with the nuber of the LiBs is one of the major obstacles. Conventional LIBs using an organic liquid electrolyte have various issues such as combustion and explosion. As a solution to these safety problems, all-solid-state lithium ion batteries are considered as candidates for advanced lithium ion batteries, which have high electrochemical stability and excellent safety due to their nonflammability of intrinsic inorganic solid electrolyte.

The solid electrolyte is the key material for the all-solid-state batteries, and that is required properties such as thermal stability, chemical durability, mechanical strength and high ionic conductivity. Sulfide based materials, such as crystalline $Li_{10}GeP_2S_{12}$,[2,3] Li_6PS_5Cl,[4] and $Li_2S-P_2S_5$ glass-ceramics[5–7] are the best candidates for the solid electrolyte systems due to their high lithium ion conductivity comparable to liquid electrolytes. Among them, the $Li_2S-P_2S_5$ glass-ceramics system exhibits a high lithium ion conductivity of $10^{-2} - 10^{-4}$ S cm^{-1} at room temperature. The $Li_2S-P_2S_5$ glass-ceramics system has a ductility that results in a large contact area between the solid electrolytes and the electrode active materials because of the easy deformation of solid electrolytes.[8]

In conventional LIBs, liquid electrolyte fills the voids within porous cathode thick films and makes good interfacial contact on the entire surface of the active materials, thus maintaining sufficient ion conduction pathways. In contrast, the all-solid-state battery uses the composite electrode structure that consists of the active materials, conductive agents and solid electrolytes. The composite cathodes are fabricated with a uniaxial cold press that is not perfectly occupied by solid materials.[6,8] Thus, it is difficult to obtain sufficient contact area between the active materials and the solid electrolytes in the cathode layer because of the specific size and rigidity of the solid electrolytes. The lack of ion conduction paths has limited the electrochemical performances of the all-solid-state batteries due to the insufficient contact area between active materials and solid electrolytes in the composite

cathode. To improve the electrochemical performances of all-solid-state batteries, some design issues of the composite electrode need to be solved. In previous work, we investigated the effect of fine sized glass-ceramics solid electrolyte powders in composite cathodes for a higher concentration of the active materials.[9] Such fine sized electrolyte makes good contact between active materials and solid electrolytes. The properties of the formed ceramic green bodies are strongly influenced by the size and the shape of ceramic powder.

In this study, the packing density of the composite cathode was improved using the bimodal sized electrolyte mixture. The particle size distributions of the fine (d_{50}: 2.548 μm) and coarse (d_{50}: 14.21 μm) solid electrolyte powders had the same ionic conductivity (8.5×10^{-4} S cm^{-1}). In powder packing theory, a ceramic body of packed discrete sized powders has a higher packing density than that of the packed uniform powders since the small powders filling the voids between large powders.[10–12] Thus, the voids in the composite cathode were filled with fine sized solid electrolyte, and the composite cathode demonstrated a decreased pore ratio (<15 vol.%) and an increased density. As a result, the all-solid-state batteries using the bimodal sized electrolyte was achieved a lower interface resistance and a large contact areas between the solid electrolyte and the cathode material, resulting in enhanced electrochemical performances.

Experimental

The solid electrolyte of the $78Li_2S \cdot 22P_2S_5$ glass-ceramics was prepared by a mechanical milling process with subsequent heat-treatment under Ar atmosphere. The starting materials of reagent-grade Li_2S (99.9%, Alfa Aesar) and P_2S_5 (99%, Sigma-Aldrich) were mixed in the appropriate molar ratios. The mixture was amorphized by a high energy planetary ball mill (Pulverisette 7, Fritsch) at 520 rpm for 30 h in a ZrO_2 pot with ZrO_2 balls with a 3 mm diameter. The amorphized glass was annealed to make a glass-ceramics using a tube furnace with high purity Ar gas (99.9999%) at 215°C. The solid electrolyte powder prepared in this process will be called the "coarse" solid electrolyte.

To make the "fine" solid electrolyte, the coarse electrolyte was pulverized by a wet ball mill process. The coarse solid electrolyte powders were dispersed in anhydrous heptane (99%, Sigma-Aldrich) and anhydrous dibutyl ether (99.3%, Sigma-Aldrich) solution. The sulfide based solid electrolyte powder is stable against both solvents.[9,13] The volume ratio of the heptane:dibutyl ether was 8:1 and the solvent to

[z]E-mail: dwshin@hanyang.ac.kr

powder weight ratio was 1:9. ZrO_2 balls with a 3 mm diameter were added with a ball-to-powder weight ratio of 30:1. The milling process for the pulverization was conducted at 200 rpm for 24 h then dried at 120°C.[9]

To evaluate the crystalline structure of both samples, X-ray diffraction (XRD) patterns of the samples were obtained with an X-ray diffractometer (Rigaku, Ultima IV) with Cu-Ka radiation (λ = 1.542 Å). To avoid air exposure, the electrolyte samples were sealed in an airtight container covered with a polyimide film and mounted on the X-ray diffractometer.

The ionic conductivities of the samples were measured using an electrochemical impedance analyzer (Wonatech, SP5) in the frequency range of 0.1 Hz – 1 MHz. The samples were pelletized under a pressure of 370 MPa with a uniaxial press, producing pellets of 13 mm diameter and a thickness of ∼1 mm. The pressed pellet was placed in a mold made from polyether ether ketone. Two stainless steel rods used as blocking electrodes which were placed above and below the pellet, respectively.

The composite cathode mixture was prepared by mixing $LiNbO_3$-coated $LiNi_{0.6}Co_{0.2}Mn_{0.2}O_2$ (NCM622), the solid electrolytes and the conductive agent (Super-P carbon, TIMCAL) with mortar and pestle at a weight ratio of 70:28:2. The composite cathode pellets of 13 mm diameter were prepared using uniaxial cold press technique that applied 370 MPa of pressure for 5 min. Cross-sectional surfaces images of the composite cathodes were prepared by ion polishing at 6 kV for 3 h with an Ar ion beam (FE-SEM, Regulus 8100, Hitachi, Japan).

The porosity of the composite cathodes can be calculated using the equation;[14]

$$\%Porosity = \left(1 - \frac{V_{true}}{V_{bulk}}\right) \times 100 \quad [1]$$

The bulk volume (V_{bulk}), including the particle and the pore volume, was calculated as a cylindrical structure using the diameter and the height of the composite cathode pellets as measured by a Vernier caliper. The true volume (V_{true}) of the composite cathode was measured using a gas pycnometer (Accupyc 1330, Micromeritics) under a high purity He atmosphere at room temperature. Volume fraction of the voids was calculated by comparing the calculated bulk volume and the measured true volume.

Brunauer-Emmett-Teller (BET) measurement of the solid electrolytes and the active materials (NCM622) were conducted with a Micromeritics 3Flex installed at the Hanyang LINC+ Analytical Equipment Center (Seoul) to confirm the surface area of the powders. To measure the contact area between the active materials and the solid electrolytes, galvanostatic intermittent titration technique (GITT) measurements were carried out with a pulse current of 0.1C for 10 min and rested for 30 min. The contact area between the NCM 622 active materials and the solid electrolyte was calculated using the following equation of the GITT measurements.[15,16]

$$D = \frac{4}{\pi\tau}\left(\frac{m_{NCM}V_M}{M_{NCM}S}\right)^2\left(\frac{\Delta E_s}{\Delta E_t}\right)^2 \quad [2]$$

Here, D is the chemical diffusion coefficient of NCM622 (1.72 × 10^{-11} cm^2 s^{-1}), S is the contact area between the solid electrolytes and the electrode active materials, τ is the pulse duration (600 s), ΔE_s is the steady state voltage change, ΔE_t is the transient voltage change, M_{ncm} is the molecular weight of the host, $Ni_{0.6}Co_{0.2}Mn_{0.2}O_2$ (90.13g mol^{-1}), m_{ncm} is the mass of the host in the sample (varied depending on the mass loading) and V_m is the molar volume of the sample (the value used for $LiNi_{1/3}Co_{1/3}Mn_{1/3}O_2$, 20.29 cm^3 mol^{-1}). The surface coverage of the solid electrolyte on the active material was obtained by dividing the specific surface area of the active material measured by BET in the composite cathode by the achieved contact area between the NCM 622 active materials and the solid electrolytes.

For cell assembly, the composite cathode mixture (15 mg) was pressed together with $78Li_2S \cdot 22P_2S_5$ glass-ceramics solid electrolyte (150 mg) as an electrolyte layer under 370 MPa pressure for 5 min. Indium foil (99.99%, Nilaco Corporation, t = 0.1 mm) as a negative
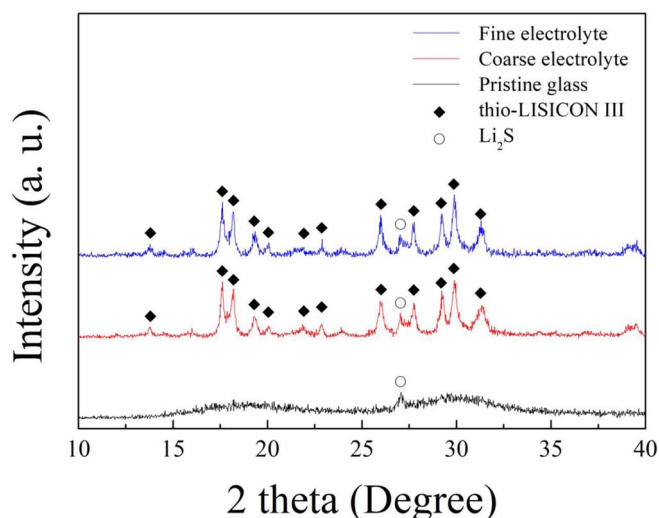

Figure 1. XRD patterns of the pristine and the milled electrolyte powders.

electrode was attached to the opposite side. The obtained three-layer pellet was fabricated into a mold-type cell. All processes were conducted in a glove box ([H_2O] < 1 ppm) with high purity (99.9999%) Ar. And the cell performance was investigated at room temperature by a charge-discharge measurement device (TOSCAT-3100, Toyo System, Japan) at room temperature. The charge–discharge performance was achieved with cut off voltages of 2.38–3.68 V (vs. Li–In) with 0.05C to 1.0 C current densities. Electrochemical impedance spectroscopy measurements of the prepared cells were performed using an impedance analyzer (Wonatech, SP5) in the frequency range of 0.001 Hz to 1 MHz after charging to 3.68 V (vs. Li–In) after first charge.

Results and Discussion

A $78Li_2S \cdot 22P_2S_5$ glass-ceramics electrolyte was synthesized by a mechanical milling technique and a subsequent heat-treatment process. Figure 1 is the XRD patterns of the coarse, fine glass-ceramics electrolytes and pristine glass. The pristine glass had a halo pattern of the glass structure and the Li_2S residue. To achieve fine powder, we conducted wet ball mill process with heptane and dibutyl ether liquid[9] which was not reacted with sulfide electrolyte due to their low polarity index.[13] The coarse and fine electrolyte powders demonstrated the same pattern as the thio-LISICON III analogue glass-ceramics[17,18] without phase deformation.[9] Figure 2 is the Nyquist plot of the coarse and fine solid electrolytes. Both the electrolytes presented the same intercept values on the x-axis, which means the same resistance value. As this result, the glass-ceramics structure of the electrolyte was maintained during the pulverization process, and the ionic conductivity of the solid electrolyte did not exhibit any electrochemical degradation as reported in a previous study.[9]

Size distributions of the powders are summarized in Table I and Figure 3. The coarse solid electrolyte powders had an average size of 14.12 μm and a broad size distribution. The fine solid electrolyte powders had an average size of 2.548 μm with a narrow size distribution. The size of the fine solid electrolyte powders was significantly reduced by the pulverization process. NCM622 cathode active material powders had a moderate average size of 6.92 μm. The surface area per unit mass of the fine electrolyte particles was approximately 4.33 times higher than the coarse electrolyte particles which was expected to increase the contact area between the active material and the solid electrolyte in the composite cathode structure. The Super-p conductive agent was reported to be 40 nm in size[19,20] which was not detected during the measurement.

Schematic models of the composite cathode with both solid electrolyte powders are presented in Figure 4. Figure 4a shows insufficient
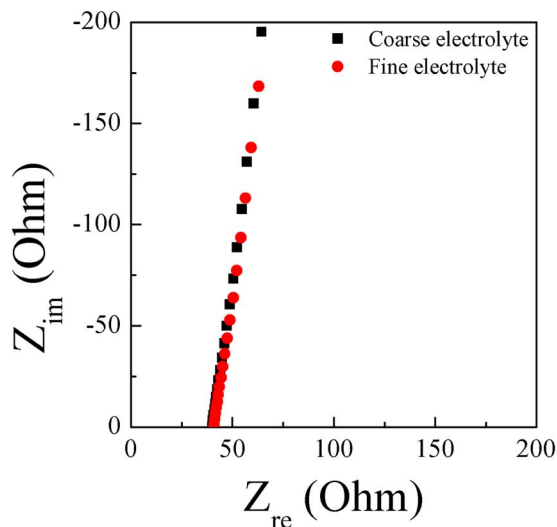
Figure 2. Nyquist plot of the coarse and fine solid electrolyte.

Figure 3. Size distribution of powders in composite cathode.

contact between the solid electrolyte and the active material. However, the composite cathodes with the fine electrolyte powders have higher contact areas in Figure 4b and Figure 4c. The microstructures of the composite cathodes are shown in Figure 5. In the Figure 5, the white area is the NCM622 cathode active materials. The gray area is the sulfide solid electrolytes with brightness change due to the contamination. The sulfide electrolytes in the composite cathode was reacted with the oxygen in the air during the loading process before FE-SEM observation. The conductive agents were well distributed in solid electrolyte area.[21] However, Super-P was not observed because it had a very small size of 40 nm.[19,20] Sample 1, consisting of only coarse electrolytes, included the large sized voids ($< 20 \mu m$ diameter), as suggested in Figure 4a. Figure 5b an Figure 5c was demonstrated the voids like cracks ($< 10 \mu m$ length). The fine electrolytes filled voids between the coarse electrolytes which was insufficient. Figure 5d and Figure 5e were demonstrated the reduced voids in composite cathode, and the surface of the active materials was covered with the electrolyte powders. In packing density theory, the composite packing density using bimodal sized powders is increased due to filling of voids with fine sized powders, as presented in Figure 4b. Thus, the data shown in Figure 5 is matched well packing density theory and the suggested model in Figure 4.
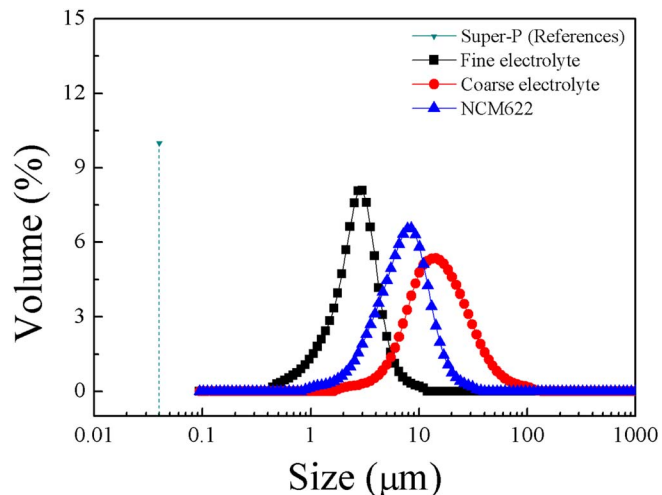
To evaluate the volume fraction of the voids in the composite cathode, the true densities and the bulk density of the composite cathode samples were measured with a pycnometer and are shown in Figure 6. The composite cathodes were prepared with a different weight ratio of the fine and coarse electrolytes. The porosity of the composite cathode pellets was calculated by Equation 1 and the entire samples had a porosity of less than 15 vol.%. Since both electrolytes are the same material with different sizes, the volume ratio of the fine and coarse solid electrolytes is assumed to follow the weight ratio of the solid electrolytes. Nevertheless, Sample 4 using a bimodal mixture had the highest densities due to reduce the voids as shown in Figure 5, which was well matched with previous studies.[16,22]

The discharge profiles from the first cycle of the GITT experiments are presented in Figure 7. The charging and discharging process is conducted at 1/10 C rate. The contact area between the active materials and the solid electrolytes was calculated by Equation 2 and is summarized in Table II. The contact area has a relationship with the composite cathode density as presented in Figure 6 because the voids in the composite cathode restricted the solid-solid particle contact. Sample 1 using the coarse electrolyte, had the lowest capacity and a minimal contact area. On the other hand, Sample 5 showed a large contact area and a higher capacity which matched pervious study.[9] Sample 4, using bimodal sized electrolyte, achieved the highest

Table I. Physical properties of active material and solid electrolytes.

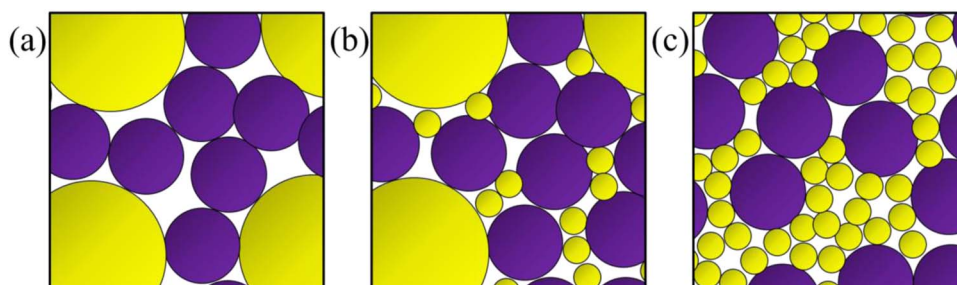| Samples	d_{10} (μm)	d_{50} (μm)	d_{90} (μm)	BET surface area (m^2 g^{-1})	Ionic conductivity (S cm^{-1})
NCM622 (LiNi$_{0.6}$Co$_{0.2}$Mn$_{0.2}$O$_2$)	3.06	6.92	12.98	0.1922	
Coarse electrolyte	6.40	14.12	33.35	1.6653	8.5×10^{-4}
Fine electrolyte	1.169	2.548	4.36	7.2097	8.5×10^{-4}

Figure 4. Schematic model of the composite cathode structure: (a) coarse electrolyte used, (b) bimodal electrolyte mixture used, (c) fine electrolyte used (yellow: solid electrolyte, purple: cathode active material).
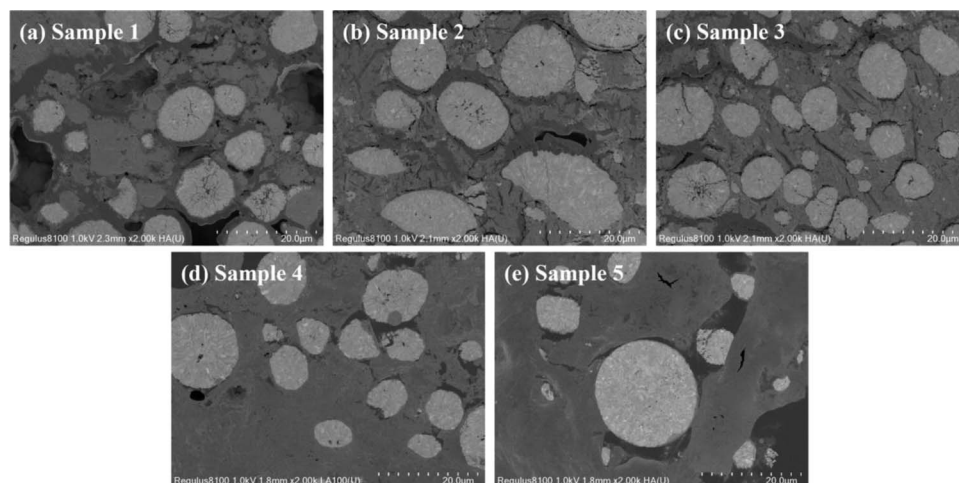
Figure 5. Cross-sectional SEM image of composite cathode samples: (a) Sample 1, (b) Sample 2, (c) Sample 3, (d) Sample 4, (e) Sample 5.
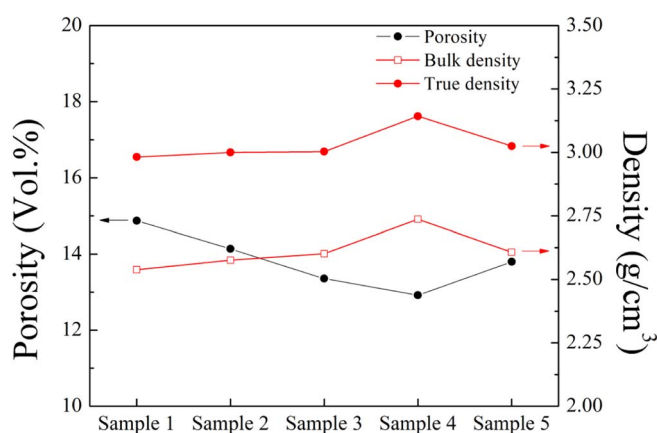

Figure 6. Density and porosity of the composite cathode samples.

Figure 7. GITT measurement data of the composite cathode samples.

capacity and the largest contact area because it had the highest density of the composite cathodes, as presented in Figure 5 and Figure 6. This result means that the bimodal sized electrolyte improved the electrochemical performances of the all-solid-state battery due to the greater density and contact area.

Nyquist plots of the composite cathode samples in Figure 8 show a semicircle and a Warburg tail. The intercept values on the x-axis are the resistance of the solid electrolyte layer, and a Warburg tail at low frequency demonstrate the Li-ion diffusion in the active materials. The semicircle at the high- to mid-frequency range is affected by the charge transfer resistance of interfaces between the active materials and the solid electrolytes. This result, the resistance was inversely proportional to the contact area as summarized in Table II. The resistance decreased with increasing weight fraction of the fine electrolyte and the bimodal
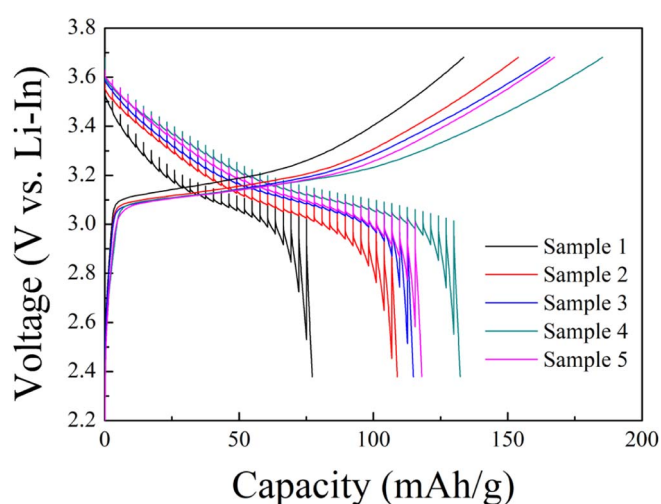
sized electrolyte. Thus, the higher resistance of Sample 1 compared to Sample 4 could be explained by the volume fraction of the voids and a lack of the contact area.

The rate capabilities of all-solid-state batteries using various samples are shown in Figure 9. The capacity of the samples at the 1/10 C rate matched well the result of GITT analysis as presented in Figure 7. The cell of Sample 1 exhibited the lowest capacity of 108.64 mAh·g^{-1} for the first discharge at 1/10 C and its capacity of 13.85 mAh·g^{-1} after 20 cycles at 1 C was due to the high volume fraction of voids, which limited the ion conduction paths in the composite cathode as shown in Figure 5. At the higher discharge rates, more lithium ions were needed to achieve a sufficient ion

Table II. Properties of composite cathode samples.

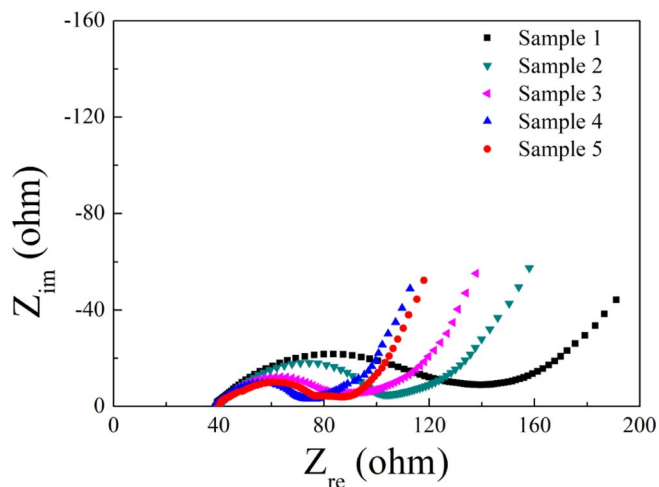| Sample name	NCM622 (wt%)	Fine electrolyte (wt%)	Coarse electrolyte (wt%)	Conductive agent (wt%)	True density (g cm^{-3})	Contact area (%)[a]
Sample 1	70	0	28	2	2.98	39.32
Sample 2	70	7	21	2	3.00	46.46
Sample 3	70	14	14	2	3.00	46.70
Sample 4	70	21	7	2	3.14	62.04
Sample 5	70	28	0	2	3.02	50.03

[a]Obtained by GITT analysis.

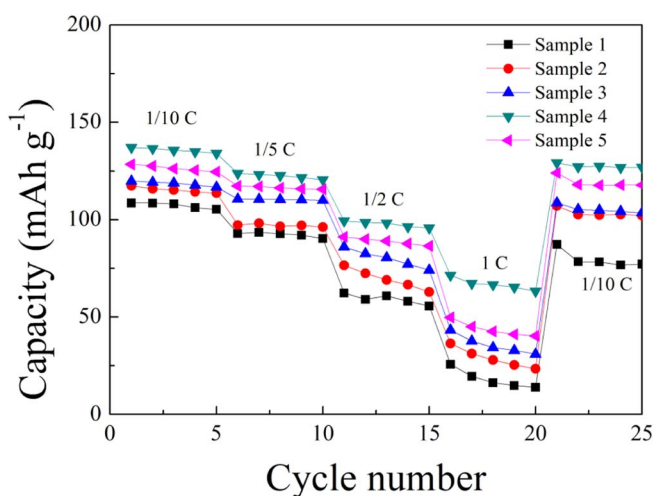**Figure 8.** Nyquist plot of the all-solid-state NCM622/In half cells.

Figure 9. Rate capability of the cells using the composite cathode.

conduction path way. In contrast, Sample 4 had the highest rate performance because it had the largest contact area and the highest density of composite cathode samples, which led to the highest capacity of 137.14 mAh·g^{-1} for the first discharge at 1/10 C and its capacity of 63.28 mAh·g^{-1} after 20 cycles at 1 C. This result demonstrated that the contact area and density of the composite cathode is the key to improving the all-solid-state battery performances, as reported in previous studies.[9,16,23,24]

Conclusions

In this report, we present the relation between a packing density of composite cathode and electrochemical performances of the all-solid-state batteries. We prepared electrolyte powders of different sizes with average electrolyte powders sizes of 2.548 μm and 14.12

μm, respectively, and the ionic conductivities of both powders were the same. The composite cathode with well-mixed the bimodal sized electrolyte minimized the voids and maximized the packing density of the composite cathode. Thus, the electrochemical performances of an all-solid-state battery with 70:7:21:2 weight ratio of the active material, coarse electrolyte, fine electrolyte and conductive agent were significantly improved due to the large contact area between the cathode active materials and the solid electrolytes. Electrochemical impedance spectroscopy indicated that the interface resistance was related to the contact area between the cathode active materials and the solid electrolytes. Finally, the good rate capability of the all-solid-state batteries with bimodal sized electrolyte was demonstrated to result from the low resistance and the minimization of the voids.

ORCID

Dongwook Shin https://orcid.org/0000-0002-8829-9638

References

1. J. M. Tarascon and M. Armand, *Nature*, **414** 359 (2001).
2. N. Kamaya, K. Homma, Y. Yamakawa, M. Hirayama, R. Kanno, M. Yonemura, T. Kamiyama, Y. Kato, S. Hama, K. Kawamoto, and A. Mitsui, *Nature Materials*, **10** 682 (2011).
3. Y. Kato, S. Hori, T. Saito, K. Suzuki, M. Hirayama, A. Mitsui, M. Yonemura, H. Iba, and R. Kanno, *Nature Energy*, **1** 16030 (2016).
4. H. J. Deiseroth, S. T. Kong, H. Eckert, J. Vannahme, C. Reiner, T. Zaiß, and M. Schlosser, *Angewandte Chemie - International Edition*, **47**(4), 755 (2008).
5. T. Ohtomo, A. Hayashi, M. Tatsumisago, Y. Tsuchida, S. Hama, and K. Kawamoto, *Journal of Power Sources*, **233** 231 (2013).
6. J. Kim, M. Eom, S. Noh, and D. J. E. M. L. Shin, **8**(2), 209 (2012).
7. K. Minami, A. Hayashi, and M. Tatsumisago, **94**(6), 1779 (2011).
8. A. Sakuda, A. Hayashi, and M. Tatsumisago, *Scientific Reports*, **3** 2261 (2013).
9. S. Noh, W. T. Nichols, C. Park, and D. Shin, *Ceramics International*, **43**(17), 15952 (2017).
10. D. C. C. Lam and M. Nakagawa, *Journal of the Ceramic Society of Japan*, **102**(1182), 133 (1994).
11. C. C. Furnas, *Industrial & Engineering Chemistry*, **23**(9), 1052 (1931).
12. X. Ye, Y. Li, Y. Ai, and Y. Nie, *Advanced Powder Technology*, **29**(9), 2280 (2018).
13. K. Lee, S. Kim, J. Park, S. H. Park, A. Coskun, D. S. Jung, W. Cho, and J. W. Choi, *Journal of the Electrochemical Society*, **164**(9), A2075 (2017).
14. J. V. Link, G. Tribuzi, and J. B. Laurindo, *LWT*, **84** 717 (2017).
15. Y. J. Nam, D. Y. Oh, S. H. Jung, and Y. S. Jung, *Journal of Power Sources*, **375** 93 (2018).
16. D. H. Kim, D. Y. Oh, K. H. Park, Y. E. Choi, Y. J. Nam, H. A. Lee, S.-M. Lee, and Y. S. Jung, *Nano Letters*, **17**(5), 3013 (2017).
17. J. Kim, Y. Yoon, J. Lee, and D. Shin, *Journal of Power Sources*, **196**(16), 6920 (2011).
18. F. Mizuno, A. Hayashi, K. Tadanaga, and M. Tatsumisago, *Solid State Ionics*, **177**(26), 2721 (2006).
19. X.-h. Yang, P. He, and Y.-y. Xia, *Electrochemistry Communications*, **11**(6), 1127 (2009).
20. I. Cho, J. Choi, K. Kim, M.-H. Ryou, and Y. M. Lee, *RSC Advances*, **5**(115), 95073 (2015).
21. S. Noh, W. T. Nichols, M. Cho, D. J. J. o., and E. Shin, **40**(4), 293 (2018).
22. K. H. Park, D. Y. Oh, Y. E. Choi, Y. J. Nam, L. Han, J.-Y. Kim, H. Xin, F. Lin, S. M. Oh, and Y. S. Jung, **28**(9), 1874 (2016).
23. A. Sakuda, A. Hayashi, T. Ohtomo, S. Hama, and M. Tatsumisago, *Journal of Power Sources*, **196**(16), 6735 (2011).
24. H. K. Tian and Y. Qi, *Journal of the Electrochemical Society*, **164**(11), E3512 (2017).